AIDA

Advanced European Infrastructures for Detectors at Accelerators

Milestone Report

First Test Results on Selected Components

Canfer, S. (STFC)

et al

01 November 2013

The research leading to these results has received funding from the European Commission under the FP7 Research Infrastructures project AIDA, grant agreement no. 262025.

This work is part of AIDA Work Package **8: Improvement and equipment of irradiation and test beam lines**.

The electronic version of this AIDA Publication is available via the AIDA web site <http://cern.ch/aida> or on the CERN Document Server at the following URL: <http://cds.cern.ch/search?p=AIDA-MS32>

Grant Agreement No: 262025

AIDA

Advanced European Infrastructures for Detectors at Accelerators

Seventh Framework Programme, Capacities Specific Programme, Research Infrastructures, Combination of Collaborative Project and Coordination and Support Action

MILESTONE REPORT

FIRST TEST RESULTS ON SELECTED COMPONENTS

MILESTONE: MS32

Document identifier:	AIDA-Mil-MS32
Due date of milestone:	End of Month 30 (July 2013)
Report release date:	01/11/2013
Work package:	WP8: Improvement and equipment of irradiation and test beam lines
Lead beneficiary:	STFC
Document status:	Final

Abstract:

In order to qualify certain materials, components and sensors for the high radiation environments that LHC detector upgrades represent, a series of tests are planned led by the partners in AIDA WP8.4. This milestone report presents initial results. The results of these and other relevant tests will be loaded into a database that is being written as a parallel activity within WP8.4.

Copyright © AIDA Consortium, 2013

Copyright notice:

Copyright © AIDA Consortium, 2013
For more information on AIDA, its partners and contributors please see www.cern.ch/AIDA

The Advanced European Infrastructures for Detectors at Accelerators (AIDA) is a project co-funded by the European Commission under FP7 Research Infrastructures, grant agreement no 262025. AIDA began in February 2011 and will run for 4 years.

The information herein only reflects the views of its authors and not those of the European Commission and no warranty expressed or implied is made with regard to such information or its use.

Delivery Slip

	Name	Partner	Date
Authored by	S Canfer, M Menichelli, C Meroni, F Nessi-Tedaldi	STFC INFN ETHZ	21/10/13
Edited by	S Canfer	STFC	25/10/13
Reviewed by	M Moll [WP coordinator] L Serin [Scientific coordinator]	CERN	31/10/13
Approved by	L Serin [Scientific coordinator]		31/10/13

TABLE OF CONTENTS

1. INTRODUCTION

AIDA Work Package 8.4, Qualification of materials and common database, will make a database available to the LHC community that contains links to results of relevant irradiated materials and components. In parallel the labs involved in WP8.4 are testing a range of materials, components and sensors in support of LHC upgrades. These are STFC, INFN Perugia, INFN Milano and associate member ETH Zurich. This milestone report presents initial results.

2. INITIAL RESULTS STATUS

Tests are in progress to qualify irradiated materials and components for the LHC experiment and machine upgrades. This document presents radiation work in progress at the institutes that form AIDA WP8.4.

Table 1: Progress against testing plan

Institute	Material or component	Particle type	Observable	Comments	Progress %
STFC	DGEBA-POPDA epoxy-S glass composite	electron	DMA, DSC thermal analysis	**Samples manufactured by RAL. Irradiated to 50MGy, waiting activation decay for thermal analysis**	66
STFC	DGEBF-MTPHA- S glass composite	electron	DMA, DSC thermal analysis		66
STFC	TGPAP-DETD epoxy – S glass composite	electron	DMA, DSC thermal analysis		66
STFC	CE/Epoxy blend– S glass composite	electron	DMA, DSC thermal analysis		66
STFC-Oxford-B'ham	Support rods for Optical fibres	26MeV p, cyclotron	Tensile strength, DMA	Samples irradiated, analysis in progress	50
STFC	Flexible epoxy for sensors RAL245	26MeV p, cyclotron	DMA (e.g. mech modulus, tan delta)	Samples due for irradiation in October 2013	33
STFC	Flexible epoxy for sensors RAL246	26MeV p, cyclotron	DMA (e.g. mech modulus, tan delta)	Samples due for irradiation in October2013	33
STFC	Flexible epoxy for sensors RAL247	26MeV p, cyclotron	DMA (e.g. mech modulus, tan delta)	Samples due for irradiation in October 2013	33
ETHZ	CeF	24 GeV/c p	induced absorption vs wavelength and recovery	Samples irradiated, analysis in progress	66
ETHZ	YSO	Proton	induced absorption vs wavelength and recovery	preliminary results available, recovery studies in progress	66

ETHZ	LuYAG	Co60 gamma	“	results available	100
ETHZ	YSO	Co60 gamma	“	preliminary results available, recovery studies in progress	66
ETHZ	CeF	Co60 gamma	“	Samples due for irradiation in fall 2013	33
INFN-MI	Field Programmable Gate Arrays (FPGA)	Protons (Energy selectable in the range 20 – 180 MeV)	Device overall characterization and power absorption measurements. Single event upset and gate rupture (SUE and SEGR) evaluation.	TSL – Sweden Samples irradiated, analysis in progress	70
INFN-MI	Field Programmable Gate Arrays (FPGA)	Neutrons (Spectrum atmospheric-like up to ≈150 MeV)	Device overall characterization and power absorption measurements. Single event upset and gate rupture (SUE and SEGR) evaluation.	TSL - Sweden	0
INFN-MI	Field Programmable Gate Arrays (FPGA)	X-rays (Emax 100 keV) or Co60 gamma rays	Device overall characterization and power absorption measurements.	Lena – Italy BNL – USA Samples irradiated, analysisin progress	50
INFN-MI	Analog to Digital Converter (ADC), Multiplexer (MUX), Clock Generators and PLL	Protons (Energy selectable in the range 20 – 180 MeV)	Device overall characterization and power absorption measurements. Single event upset, gate rupture and soft error rate (SUE SEGR and SER) evaluation.	TSL - Sweden	0
INFN-MI	Analog to Digital Converter (ADC), Multiplexer (MUX), Clock Generators and PLL	Neutrons (Spectrum atmospheric-like up to ≈150 MeV)	Device overall characterization and power absorption measurements. Single event upset, gate rupture and soft error rate (SUE SEGR and SER) evaluation.	TSL - Sweden	0
INFN-MI	Analog to Digital Converter (ADC), Multiplexer (MUX), Clock Generators and	X-rays (Emax 100 keV) or Co60 gamma rays	Device overall characterization and power absorption measurements.	Lena – Italy BNL – USA Samples irradiated, analysis in progress	60

	PLL				
INFN-MI	Custom designed Application Specific Integrated Circuits (ASICs)	Protons (Energy selectable in the range 20 – 180 MeV)	Device overall characterization and power absorption measurements. Single event upset and gate rupture (SUE and SEGR) evaluation.	TSL - Sweden	0
INFN-MI	Custom designed Application Specific Integrated Circuits (ASICs)	Neutrons (Spectrum atmospheric-like up to ≈150 MeV)	Device overall characterization and power absorption measurements. Single event upset and gate rupture (SUE and SEGR) evaluation.	TSL - Sweden	0
INFN-MI	Custom designed Application Specific Integrated Circuits (ASICs)	X-rays (Emax 100 keV) or Co60 gamma rays	Device overall characterization and power absorption measurements.	Lena – Italy BNL - USA	0
INFN-MI	Power Mosfet (Si and GAN)	Protons (Energy selectable in the range 20 – 180 MeV)	Device overall characterization and power absorption measurements. Single event upset and gate rupture (SUE and SEGR) evaluation.	TSL – Sweden Samples irradiated, analysis in progress	50
INFN-MI	Power Mosfet (Si and GAN)	Neutrons (Spectrum atmospheric-like up to ≈150 MeV)	Device overall characterization and power absorption measurements. Single event upset and gate rupture (SUE and SEGR) evaluation.	TSL - Sweden	0
INFN-MI	Power Mosfet (Si and GAN)	X-rays (Emax 100 keV) or Co60 gamma rays	Device overall characterization and power absorption measurements.	Lena – Italy BNL – USA Samples irradiated, analysis in progress	80
INFN-MI	DC-DC converter an Point of Load (POL)	Protons (Energy selectable in the range 20 – 180 MeV)	Device overall characterization and power absorption measurements. Single event upset and gate rupture (SUE and SEGR) evaluation.	TSL – Sweden Samples irradiated, analysis in progress	50

INFN-MI	DC-DC converter an Point of Load (POL)	Neutrons (Spectrum atmospheric-like up to ≈150 MeV)	Device overall characterization and power absorption measurements. Single event upset and gate rupture (SUE and SEGR) evaluation.	TSL - Sweden	0
INFN-MI	DC-DC converter an Point of Load (POL)	X-rays (Emax 100 keV) or Co60 gamma rays	Device overall characterization and power absorption measurements.	Lena – Italy BNL – USA Samples irradiated, analysis in progress	80
INFN-PG 1	Si pixel module (analog readout)	X-rays (Emax 100 keV)	Characterization of detector and readout electronics	CMS	5
INFN-PG 2	Si pixel module (analog readout)	Protons (63 and/or 14 MeV)	Characterization of detector and readout electronics	CMS	0
INFN-PG 3	Active Pixel Sensor device (analog readout) [no epi-layer]	Protons (63 MeV and/or 14 MeV)	Characterization of detector and readout electronics	RAPS	0
INFN-PG 4	Active Pixel Sensor device (analog readout) [no epi-layer]	X-rays (Emax 100 keV)	Characterization of detector and readout electronics	RAPS	5
INFN-PG 5	Industrial CMOS APS (analog readout) [very small pixel size]	X-rays (Emax 100 keV)	Characterization of detector and readout electronics	Commercial active pixel detector	5
INFN-PG 6	Industrial CMOS APS (analog readout) [very small pixel size]	Protons (63 MeV and/or 14 MeV)	Characterization of detector and readout electronics	Commercial active pixel detector	70

3. APPENDIX A: INITIAL RESULTS FROM STFC (THERMOSET POLYMER MATRICES FOR LHC UPGRADE APPLICATIONS)

3.1. INTRODUCTION

Work at STFC is focussing on formulating polymers for LHC machine and detector upgrades, characterising the materials before irradiation and qualifying these by irradiation to representative doses. The same characterisation tests will then be used to look for changes in the properties of interest.

Thermoset polymers are required for many applications in the LHC machine and detector upgrades. The requirements set for these materials are very wide, in terms of uncured and cured material properties and the cure schedules that can be accommodated. For example polymeric adhesives are required to bond large area, fragile silicon detector elements to support structures. This application requires a low modulus, flexible material to avoid applying stress to the silicon as the structure contracts due to thermal contraction. Only ambient or modest temperatures can be used for curing such adhesives. More rigid adhesives are required to bond structural parts in a more traditional sense and often higher cure temperatures may be employed before the structures are populated with sensitive detectors. Structural elements such as detector supports and structures under very high stress such as magnet systems require high modulus materials so that deformations are minimised and components are maintained in position to very high accuracy.

Appropriate formulation of polymers such as epoxies and cyanate esters is the key to addressing these issues.

Rigid structural polymers and flexible polymers are discussed separately below.

3.2. RIGID POLYMERS FOR STRUCTURAL APPLICATIONS

Epoxy materials have been widely used as composite matrix materials. Composite materials are particularly useful in particle physics where they are suited to construction of one-off structures, and can have high stiffness relative to radiation cross-section, with appropriate choice of fibres. In high radiation environments, for example at doses of over 10MGy, the limiting factor in application of these materials the radiation hardness of polymer matrices.

An alternative chemistry to epoxies is cyanate ester (CE) which has been developed for high temperature applications. The same structural features that lend high temperature endurance tend to lead to good radiation stability. Studies reported for the Toroidal Field coils of the ITER project (Weber et al, ATI Vienna) report that pure cyanate ester and blends of cyanate ester and epoxy have a high level of radiation stability when exposed to gamma and neutron doses in a fission environment.

Any thermosetting material has an exotherm associated with its curing reaction. An understanding of cyanate ester formulation is required in order to apply them safely and avoid a runaway exotherm. Two factors are important; appropriate choice of catalysts and the curing time-temperature profile (cure schedule), therefore a study to establish starting formulations and safe working methods has been performed at RAL. See Appendix C.

3.3. IRRADIATION OF STRUCTURAL COMPOSITES

A range of composites for structural use have been manufactured at STFC-RAL. Four chemistries were chosen to present a range of radiation hardness. These consisted of two conventional di-epoxy materials, with anhydride and long chain amine curing agents respectively; trifunctional epoxy with aromatic amine; and a cyanate ester. Sheets were produced by vacuum impregnation of 0-90 degree plain weave S-glass fabric (manufactured by SP Systems), followed by curing in a press to produce flat panels of defined thicknesses. S glass was chosen because it is free from Boron, whereas the more conventional E-glass has Boron present as oxides to perform a flux function. Boron-free E glass is becoming more widely available as of 2013. Also S glass is suitable for high temperature heat treatment necessary for niobium-tin magnets, again this is related to the lack of boron based flux agents. Thin (0.2mm nominal) panels were manufactured using vacuum impregnation for electrical breakdown testing, in a thickness that is representative of magnet insulation for example, and thicker panels were manufactured with the fibres placed at 45 degrees for tensile testing. The fibre angle was chosen such that the tensile test stresses the matrix preferentially, and changes in the properties due to radiation are measured rather than being masked by the fibres, whose properties are not expected to change.

These samples were supplied to Wroclaw University who managed the irradiation and performed some testing (NB outside the AIDA work package, which is not presented here). In this AIDA work package, thermal analysis has started using DSC and DMA methods.

Irradiation was performed at 77K, to a dose of 50MGy using 4MeV electrons. The dose was chosen to match the levels in LHC upgrade dipole magnets, and is at a level known to damage most common di-epoxy based materials which are found in most epoxy formulations. One of the epoxy formulations tested here was such an epoxy, as an example of a “control” material.

A separate structural composite material acting as a strength member for optical fibres is also being studied. This material has been tested in tension, but it proved difficult to obtain a valid result as the rod tended to slip in the grips. A lower bound obtained was 700Newtons. FTIR-ATR (Fourier Transform Infra-Red) analysis was attempted but a very low signal was obtained from the polymer component because of the very high fibre content of this material. DMA analysis in 3 point bend is in progress.

3.4. FLEXIBLE EPOXY FORMULATIONS

A particular application for which no suitable commercial material has yet been found is the bonding of silicon sensors to support structures, such as in the ATLAS Tracker Upgrade. The radiation tolerance requirement for this application is below 1MGy. This adhesive must have low modulus so as to keep the silicon detector stress-free when the support structure deforms

due to thermal contraction or mechanical forces. The operating temperature of the detectors can be as low as -50°C. Most epoxies are not formulated to be flexible at this temperature. In general, the chemical structural features that lend flexibility (long chain length and low crosslink density) also lead to low radiation tolerance.

The extent of the sensitivity of flexible epoxies to radiation has not yet been established, and so a program of irradiation tests is in progress.

3.5. FORMULATIONS

RAL Epoxy reference	Flexibiliser PPGDGE % of resin side (balance DGEBF)	Flexibiliser POPDA-2000 % of hardener side (balance DETDA)	Accelerator AEP
245	50	10	10
246	50	30	10
247	50	50	10

The formulation consists of two epoxide resin-functional materials and two amine-functional materials. This gives a very wide range of possible glass transition temperatures, from sub-zero C (with 50% resin-side flexibiliser and 50% hardener-side flexibiliser), up to 150°C (with no flexibilisers). An optional accelerator material can be added to modify the cure temperature and time. The activity of the accelerator depends on the mix, with more flexible materials typically taking longer to cure. At 10 parts by weight per hundred of total resin weight, cure completes in 24 hours at 60°C.

Radiation

Irradiation will be performed at Birmingham Cyclotron starting in August 2013 to fluences relevant for the ATLAS Tracker upgrade for 3000 fb^{-1}, 10^{15}neq/cm2 (ref. I Dawson ATL-UPGRADE-PROC-2011).

3.6. TEST METHODS

3.6.1. DMA

Dynamic Mechanical Analysis is a technique for measuring viscoelastic and dimensional changes in a material as a function of temperature and/or frequency. The DMA can measure properties of materials such as thick pastes up to very stiff fibres. It is particularly useful for measuring glass transition temperatures and thermal expansions in polymer materials.

In static, TMA, mode, very precise measurements of dimensional changes can be measured such as thermal expansion and shrinkage due to moisture loss or chemical reaction.

The Netzsch DMA 242 at RAL consists of a force motor which can apply forces of up to 24 N to a central rod; a LVDT to measure displacement; and a sample environment. A variety of

fixtures are available to transmit this oscillating force to a specimen. A temperature controlled environment is raised around the fixture. Sub-ambient temperatures are achieved using liquid or gaseous nitrogen from a 60litre pressurised Dewar. The frequency of the exciting force can be up to 50Hz and multiple frequencies can be used in one test. Force, probe position and sample temperature are recorded and converted to mechanical properties such as storage and loss moduli using sample dimensions. Changes in these properties can show phase changes in the material. In resin systems, the temperature at which the major, alpha, phase change occurs (e.g. glass transition temperature) can be used to assess the "degree of cure" of the material. Secondary phase changes can also be detected, these are associated with side-chain mobility and are found at lower temperatures than the alpha transition. DMA is highly sensitive to these changes compared to other techniques such as DSC.
For high stiffness materials, above 1GPa, 3-point bend test fixtures are used with a 10mm or 50mm span; while for very low stiffness materials a compressive fixture of diameter 3 or 15mm is suitable.

The Netzsch DMA machine was purchased in early 2013. Many calibration runs were required so that effects of load train inertia and stiffness are removed from the data for each different loading frame in use. Temperature calibration was performed using the melting points of zinc, indium and water.

A Netzsch Dielectric Analysis (DEA) module is also available at RAL to characterise higher frequencies than are available mechanically. This uses the DMA sample environment.

3.7. RESULTS

Mechanical spectra have been recorded using the DMA before irradiation between -100 and 50C at frequencies of 0.1 to 10Hz. In order to measure over the expected wide range of modulus values the test geometry must be chosen carefully. Tests have been run with 3 point bend with 10mm span and 3mm sample thickness, and compression with samples 3mm thick and probe diameters of 15 and 3mm. Compression with 3mm probe was found to give the best results, balancing the requirements of staying within the force range of the DMA and giving sufficient sample movement.

Data can be analysed in many ways using Netzsch Proteus software. The most useful form of this data is a modulus-temperature plot which gives data that designers can understand easily and use directly in FEA codes.

Results suggest that formulation 245 has a softening point rather high to be useful, around 0°C (see Figure 1). Formulation 246 has a softening point of around -30°C. Precise values depend on measurement frequency, as expected since epoxies exhibit viscoelastic properties. Figure 1 also shows that modulus climbs rapidly to a value of 3000MPa at -30°C, which is a typical value for a pure epoxy below its Tg. Modulus then increases at a lower rate as temperature drops.

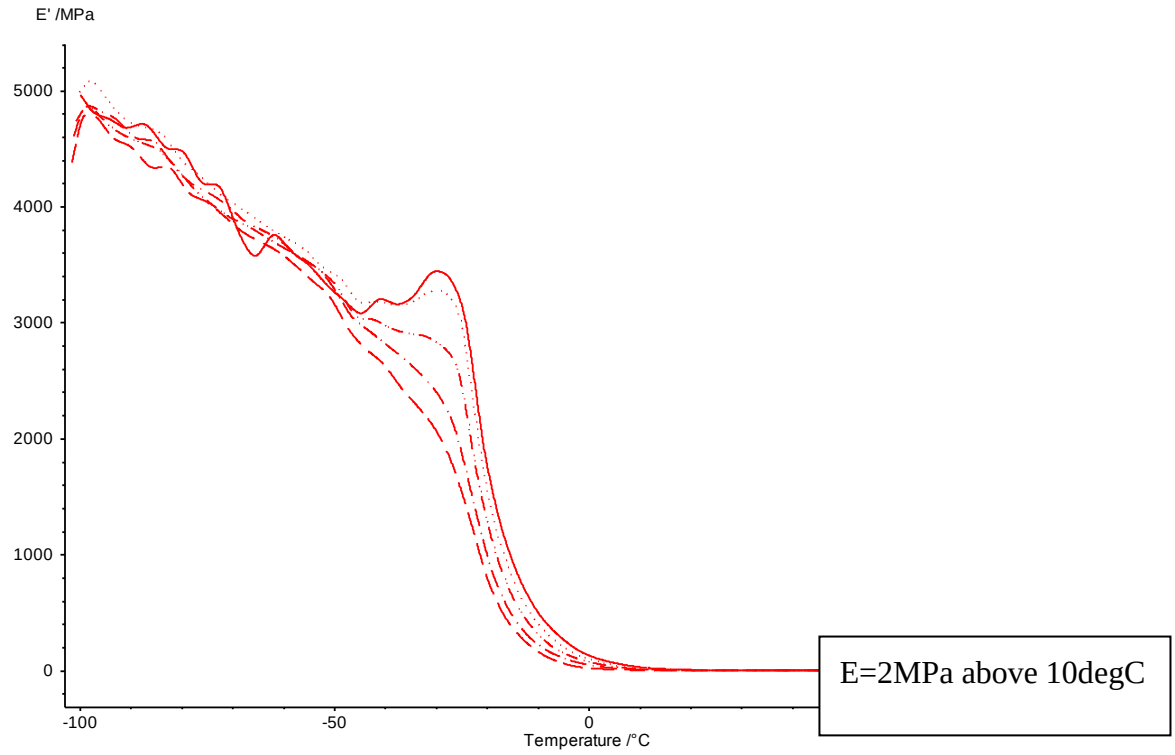

Figure 1: Typical data, Modulus vs Temperature, Flexible epoxy 245 at frequencies 1 to 20Hz

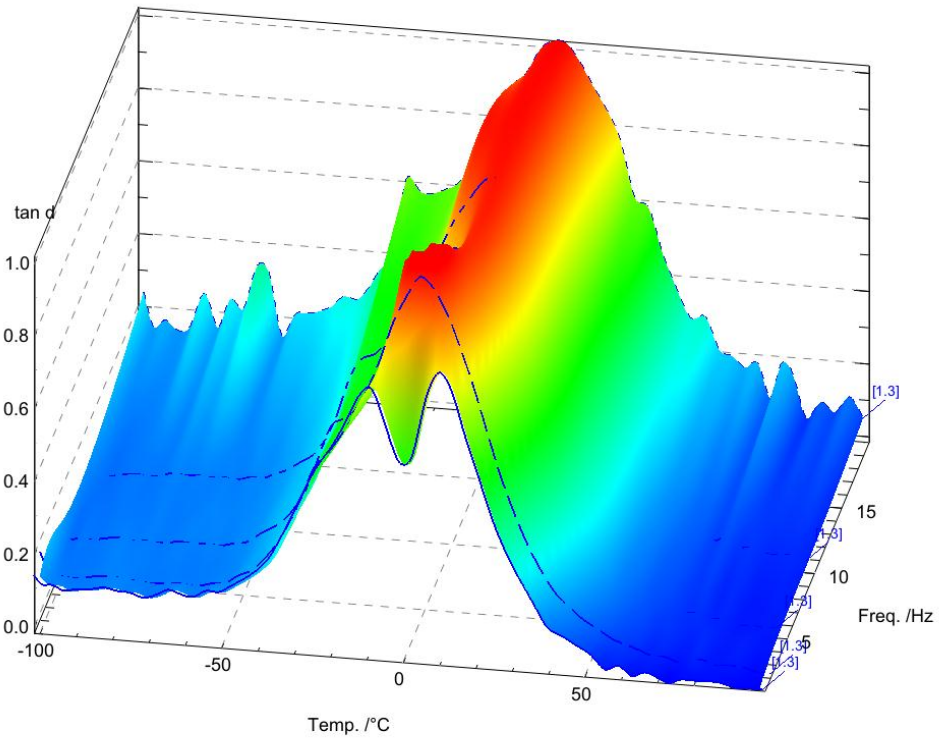

Figure 2: DMA data RAL245: tan-delta surface as a function of temperature with frequencies from 1 to 20Hz

Figure 2 shows an example of how results vary with frequency. This plot of flexible epoxy RAL245 shows two tan-delta peaks when measured at 1Hz but not at other frequencies. A secondary beta peak at -26C is visible as a shoulder at 1Hz to 10Hz, but a distinct peak at 20Hz. Samples will be re-measured and analysed to determine the effect of radiation on modulus.

Analysis of the data in the frequency domain can also give toughness information. DMA data has been compared (Woo 1994) with impact testing at low temperatures resulting in good correlation of the brittle-ductile transition temperature measurement from impact, with area under the tan-delta curve from DMA. Toughness is relevant here as an indication of resistance to crack propagation, such as could potentially occur between a silicon sensor and the substrate. So for example any reduction in the beta peak in Figure 2 could indicate a less tough material.

4. APPENDIX B: INITIAL RESULTS FROM PERUGIA (STATUS OF ACTIVITIES IN PERUGIA FOR WP 8.4, 18 JULY 2013)

4.1. PRESENT STATUS

The Perugia Group for the WP 8.4 is composed by the following researcher: Mauro Menichelli (resp.), Gian Mario Bilei, Lucia Bissi and Leonello Servoli. The tasks of this group are related with radiation testing of silicon pixel detectors as outlined in Table 1.

Table 1: status of the activities as defined in document Definition of test procedures AIDA-MS30 dated 9 March 2013, page 6

Activity no.	Component	Radiation type	Observable	Comments	Percentage of completion
1	Si pixel module	X-rays (Emax 100 keV)	Characterization of detector and readout electronics	CMS	5%
2	Si pixel module	Protons (63 MeV and/or 14 MeV)	Characterization of detector and readout electronics	CMS	0%
3	Active Pixel Sensor device (analog readout) [no epi-layer]	Protons (63 MeV and/or 14 MeV)	Characterization of detector and readout electronics	RAPS	0%
4	Active Pixel Sensor device (analog readout) [no epi-layer]	X-rays (Emax 100 keV)	Characterization of detector and readout electronics	RAPS	5%
5	Industrial CMOS APS (analog readout) [very small pixel size]	X-rays (Emax 100 keV)	Characterization of detector and readout electronics	Commercial active pixel detector	5%
6	Industrial CMOS APS (analog readout) [very small pixel size]	Protons (63 MeV and/or 14 MeV)	Characterization of detector and readout electronics	Commercial active pixel detector	70%

About the activity 6 the detectors have been irradiated and the first results of these tests have been presented at the 2 annual AIDA workshop by Leonello Servoli. The data analysis has to be finalized for this task for the remaining 30% of completion percentage.

The results presented are described in more detail in the rest of this document.

We have irradiated a standard CMOS imager (MT9V011), manufactured by Aptina Imaging, fabricated with a 130 nm technology without radiation hardening (Fig.1). This device features a VGA sensor (640x480 pixels) with 5.6x5.6μm^2 pixel size and 4.0μm thick epitaxial layer and has a built-in 10-bit ADC [1]. The irradiation was performed with the 24 MeV proton beam at INFN Laboratori Nazionali del Sud, Catania (Italy) up to a nominal fluence of 10^{14} protons/cm^2.

The sensor has been extensively characterized in the past [2-4], showing excellent performance for particle detection. Among the main findings, it should be mentioned: single pixel noise from 8 to 40 electrons of Equivalent Noise Charge (depending on the amplifier gain), dynamic range varying from 1–8 keV (highest gain) to 2–150 keV (lowest gain), Signal/Noise (Landau MPV/single pixel noise) ~30 for a Minimum Ionizing Particle (MIP), a charged particle detection efficiency for a MIP of 99.9% with a fake hit probability of less than 4x10^{-5}. Eventually, the measured spatial resolution is about 0.65 μm. To complete the characterization of the MT9V011 sensor as ionizing radiation detector, in this work we have investigated its resistance to radiation damage using the 24 MeV proton beam at the INFN LNS Laboratories (Laboratori Nazionali del Sud, Catania, Italy) using a dedicated test setup.

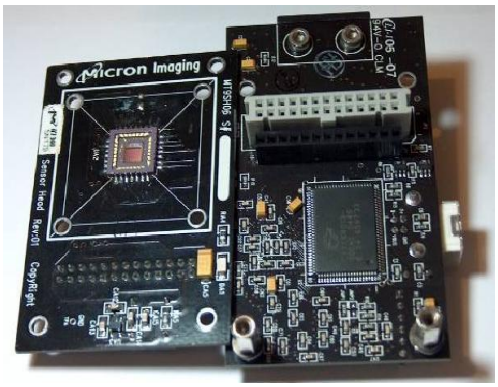

Figure 1: The MT9V011 sensor, the sensor board (left) and the DAQ board (right)

Proton irradiation at LNS (24 MeV proton beam)

A 1 mm diameter aluminium collimator, featuring a proton stopping thickness of 2 cm, has been attached to the exit beam vacuum flange (Fig. 2) to protect the device's peripheral circuit, being the goal of the test to study the radiation resistance of the single pixel and of the on-pixel electronic. The sensor evaluation board has been operated continuously during the irradiation.

The beam current used ranged from 10pA to 9.6nA, delivered in nine steps during 8 hours, doubling the current at each step, for an estimated total fluence of 10^{14} protons/cm^2. After each irradiation step, a short pedestal evaluation has been taken to measure the effects of the radiation damage on the pixel response in the absence of an external stimulus

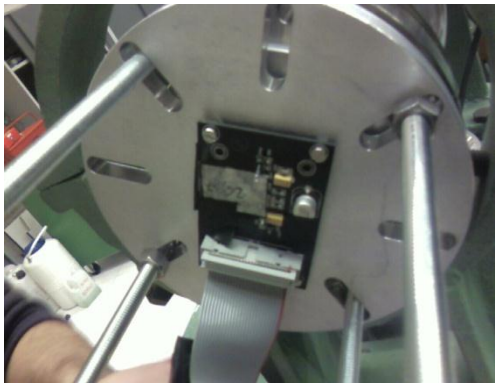

Figure 2: View of the assembled setup at LNS proton beam

The circular shape and depth of the aluminium collimator caused the creation of progressively less damaged concentric pixel rings outside the hole (Fig. 3a), with single pixel pedestal correlated to the amount of radiation damage (Fig. 3b).

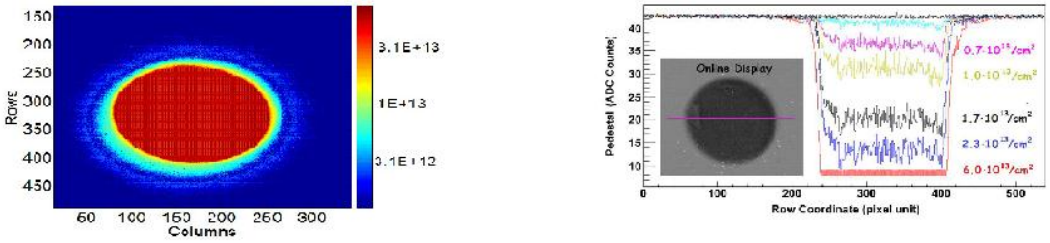

Figure 3: (a)Radiation damage mapping. (b) Pixel pedestal along a section (purple line) vs fluence

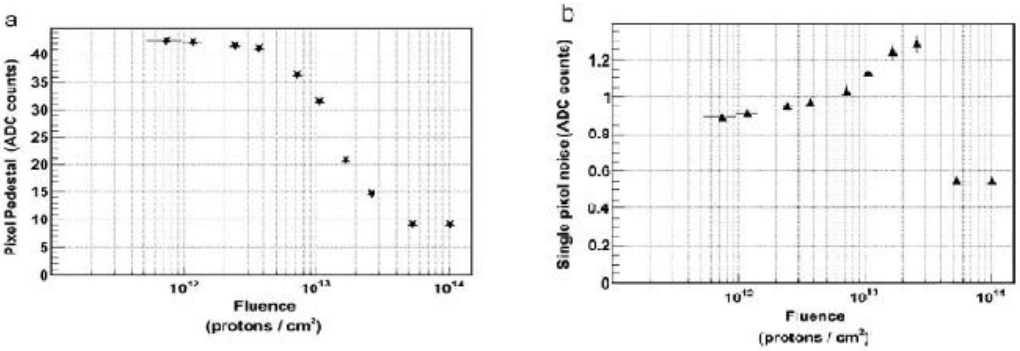

Figure 4: Evolution as a function of the fluence of (a) average pixel pedestal and (b) average single pixel noise

In fact the proton irradiation has caused two variations of the sensor performances [5]: the increase of the single pixel noise from 0.89 ADC (undamaged) to 1.2 ADC counts and the pedestal variation from 42.5 ADC to 10 ADC counts at 2.3×10^{13} protons/cm^2.

The device showed negligible damage up to 2.5×10^{12} protons/cm^2, while the pixels went almost dead (e.g., showing unrealistic noise less than 0.5 ADC counts) at 5.9×10^{13} protons/cm^2 (Figs. 4a-b).

4.2. SINGLE PIXEL RADIATION DAMAGE CLASSIFICATION

A reverse function can be then built (Fig. 5a) to correlate the fluence to the pedestal measurement of each pixel of the matrix (also the ones outside the hole). This inversion technique works properly in the range of fluence below 4×10^{13}; for fluences above this value the function becomes unsuitable for inversion purpose. Hence sets of pixels with the same damage level could be defined. The fluence interval to define each set has been chosen to have at least 50 pixels for each set (Fig. 5b). We have then studied the pixel response to monoenergetic photons as a function of their radiation damage level.

After 18 months from the irradiation damage session, with the detector stored at room temperature, a study on the photon detection efficiency and the charge collection capability has been carried out using fluorescent X-ray photons, emitted from a copper target.

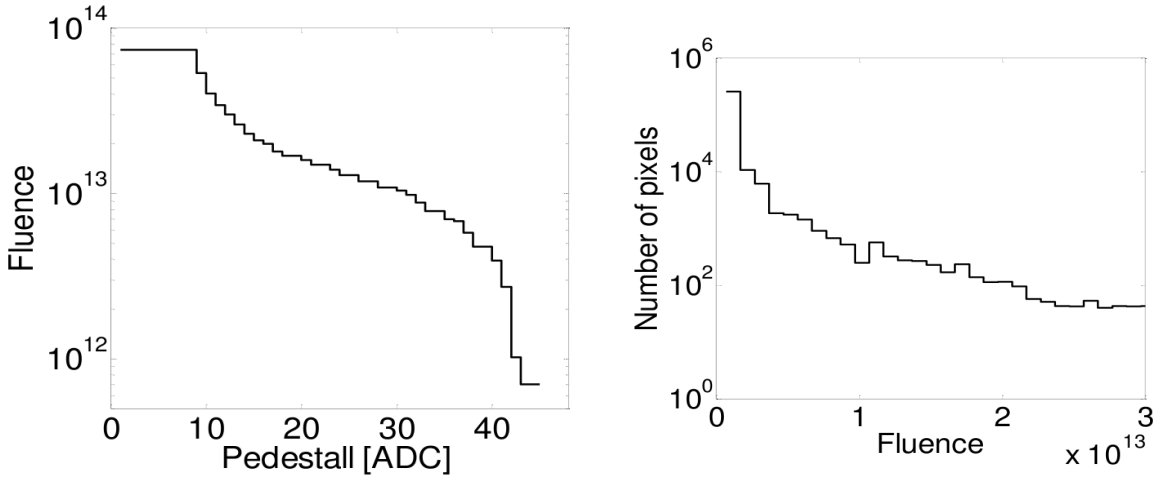

Figure 5: (a) Pedestal vs fluence correlation. (b) Number of pixels assigned to each fluence interval.

4.3. RESULTS AND DATA ANALYSIS

The charge collection efficiency has been evaluated studying the dependency on the radiation damage of the photon spectra. For each class (of comparable damaged pixels) previously

defined, the photon spectrum has been built. In the response of undamaged pixels (Fig. 6a) are clearly appreciable two peaks due to the 8.0 and 8.9 keV photons. For damaged pixels (Fig. 6b) a reduction of the collected charge occurs and a worsening of the resolution for fully contained energy deposition.

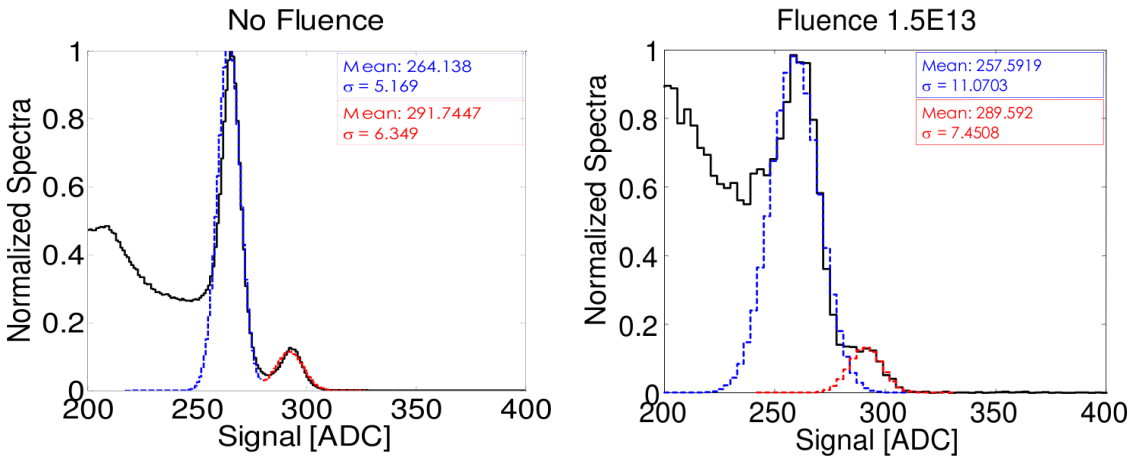

Figure 6: (a) Undamaged and (b) damaged pixel response to Cu fluorescence

Actually, the fraction of events with partial charge collection is considerably higher with respect to the undamaged pixels. In Fig. 7a is shown the evolution of S/N ratio in the detection of 8.0 keV photons as a function of radiation fluence. The S/N ratio is defined as the ratio between the peak value corresponding to 8.0 keV photons and the single pixel noise. A worsening of the S/N ratio of less than a factor two is observed, due to the loss of signal collection and also to the increase of the single pixel noise. It is worthwhile to note that this level of pixel response is still quite good for many applications and that only the damaging of the CMOS on-pixel circuitry is the limiting factor, not the damage of the sensitive element.

The photon detection efficiency has been defined as the detected number of photons per unit area for each pixel set, normalized to the same quantity measured for an undamaged region. In Fig. 7b is shown the dependence of the photon detection efficiency from the fluence. The sensor retains a reasonable capability (50%) of detecting single photons with energy of 8.0 and 8.9 keV up to a fluence of $3x10^{13}$ protons/cm^2.

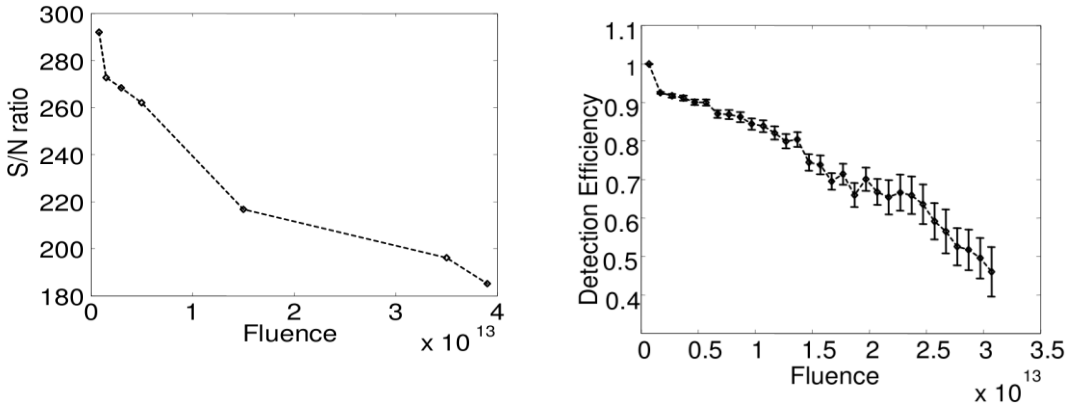

Figure 7: (a) S/N ratio vs fluence and (b) photon detection efficiency vs fluence.

4.4. CONCLUSIONS

We have investigated the radiation hardness of standard CMOS imager Micron MT9V011 up to a fluence of $4x10^{13}$ protons/cm^2 (@24MeV). The proton irradiation has caused two different type of damage: the increase of single pixel noise and the variation of the pedestal value.

Using the latter we have defined a method to evaluate the radiation damage of each pixel, making possible a pixel classification in damage classes, and the subsequent study of single pixel charge collection efficiency and photon detection efficiency.

This study shows that the damage of the sensor element is limited (less than 50% loss in both charge collection efficiency and photon detection), being the present limiting factor the radiation hardness of CMOS on-pixel circuitry. Hence commercial CMOS imagers can be fit for some applications where ionizing radiations with moderate radiation damage are involved.

4.5. REFERENCES

Aptina Imaging, MT9V011 Data Sheets.

L. Servoli et al.,*Characterization of Standard CMOS Pixel Imagers as Ionizing Radiation Detector*, JINST 5 P07003 (2010) 001-013.

L. Servoli et al., *Use of standard CMOS imagers as position detectors for charged particle*, Nucl. Phys. B-Proc. Suppl. 215 (2011) 228-231, DOI: 10.1016/j.nuclphysbps.2011.04.016.

S. Meroli et al., *A grazing angle technique to measure the charge collection efficiency for CMOS active pixel sensors*, Nucl. Instr. and Meth. A 650 (2010) 230-234, doi:10.1016/j.nima.2010.12.122.

L. Servoli et al., *Continuous measurement of radiation damage of standard CMOS imagers*, Nucl. Instr. and Meth. A 658 (2011) 137–140

5. APPENDIX C: STATUS OF ACTIVITIES AT ETH ZURICH

5.1. INTRODUCTION

ETH Zurich is studying inorganic, scintillating materials that could be used for calorimetry at the upgraded High-Luminosity LHC collider (HL-LHC). The needs for an upgrade are based on the observed evolution of detector performance in the actual CMS experiment, that is using Lead Tungstate scintillators. In the CMS electromagnetic calorimeter (ECAL), a dedicated series of tests performed by our group has shown that a hadron-specific, cumulative damage to the Lead Tungstate crystals has to be expected, which reduces light transmission while not affecting the scintillation mechanism. The damage is due to the extremely high-energy deposit of fragments from the fission of heavy nuclei [2.2-1 through 2.2-3]. The mechanisms intervening in the hadron-specific component of damage to Lead Tungstate have been understood by performing, in collaboration with the Mineralogy Institute of the Geneva University and the Metrology Group of CERN, dedicated irradiations and laboratory observations to visualize the regions of disorder ("fission tracks") left by energetic hadrons in Lead Tungstate, that we had predicted already in [2.2-1]. The results from this study have been published in [2.2-4].

Hadron damage is expected to progressively affect the various terms that contribute to the energy resolution, starting from large pseudo-rapidity (η) values inwards, through a reduction of signal amplitude, increased noise and increased non-uniformity of light collection, which should start becoming apparent already during the current LHC running. The anticipated evolution of performance and current R&D efforts by the CMS collaboration have been presented in [2.2-5].

Depending on the ECAL performance needed at the HL-LHC and on the evolution observed during ECAL running at the LHC, a fraction of the $PbWO_4$ crystals in CMS may need to be replaced with a different type of calorimeter in the ECAL end caps. As one of the potential substitute scintillators, we have studied Cerium Fluoride, where no production of heavy fragments is expected, since its elements lie below the fission barrier of Z=71 [2.2-6]. Our expectations have been confirmed by measurements that can be found in [2.2-7]. These reveal how in Cerium Fluoride no cumulative hadron-induced damage is observed, thus proving how CeF_3 is an extremely damage resistant crystal, well suitable for running at the HL-LHC. A further candidate for replacing at least part of the ECAL crystals for HL-LHC running is LYSO (Lutetium Yttrium Orthosilicate), which has already been measured to be quite resistant to □-radiation [2.2-8]. We have published results on LYSO hadron irradiation studies in [2.2-9], that demonstrate how LYSO is 5 times more resistant to energetic hadrons than Lead Tungstate. We have further started studying YSO (Yttrium Orthosilicate), that we expect to exhibit an even higher radiation resistance than LYSO due to the absence of Lutetium in its composition, along with some samples of scintillating ceramics we have received from the Shanghai Institute of Ceramics (SIC) in China. Such sintered materials might in fact constitute the most economic scintillating media of the future, were a sampling calorimeter to be envisaged for the ECAL upgrade.

We have recently contacted different producers of inorganic scintillators to start R&D efforts for the development and optimization of Cerium Fluoride, YSO and scintillating ceramics, with the ultimate aim of demonstrating that commercially adequate production capabilities exists.

5.2. PRELIMINARY RESULTS ON CERIUM FLUORIDE

We have received newly produced Cerium Fluoride samples from a potential supplier. A first irradiation with 24 GeV/c protons on a sample has been performed at the IRRAD1 facility of the CERN SPS in 2012, up to an integrated fluence of 10^{14} p/cm^2. The observed damage is larger than what observed in a sample from the nineties, studied in [2.2-7], and thus R&D on sample production is being continued by the manufacturer. Irradiations with ^{60}Co on different samples indicate that the damage observed might be due to the ionizing dose associated with the proton irradiation. Since such a damage is mostly due to the formation of color centers, improvements of growth conditions and raw material purity are expected to reduce this damage component and thus solve the problem.

5.3. PRELIMINARY RESULTS ON YSO

We have received YSO:Ce samples from two suppliers. Irradiations with 24 GeV/c protons have been performed at the IRRAD1 facility of the CERN SPS in 2012, up to integrated fluences of 10^{13} p/cm^2 and 10^{14} p/cm^2 respectively, in two different samples. First results are available for a sample produced by the Shanghai Institute of Ceramics (SIC), 17 mm x 15 mm x 15 mm in size. From the change in transmission after irradiation with 10^{13} p/cm^2 at the peak of scintillation emission, we obtain an induced absorption coefficient of 1 m^{-1}, similar to the values observed for Lead Tungstate, see Fig. 1.

Further results are expected for the sample irradiated up to 10^{14} p/cm^2, when residual radiation levels will have dropped sufficiently for safe handling in the laboratory.

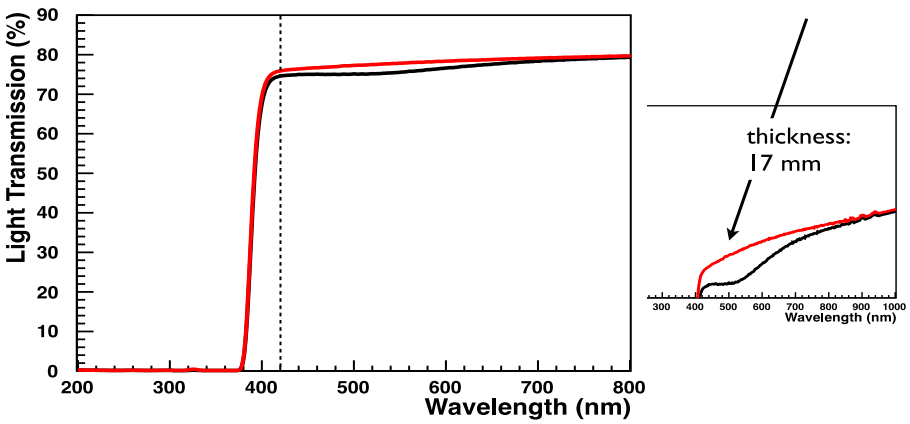

Figure 1: Light transmission for YSO:Ce as a function of wavelength before (red) and after (black) irradiation with 24 GeV/c protons up to 10^{13} p/cm^2. The arrow indicates the wavelength of maximum scintillation emission in the enlarged portion of the plot.

5.4. PRELIMINARY RESULTS ON SCINTILLATING CERAMICS

We have tested a few scintillating ceramics samples, which have been developed for purposes other than calorimetry in high-energy hadron collisions. Thus, we did not expect them a priori to be optimized in their radiation hardness. The samples have been exposed to -radiation from a ^{60}Co source, at a dose rate of 0.58 kGy/h for 65 hours for an integrated dose of 38 kGy.

All the studied samples contain Cerium as the activator for scintillation, and emit a broad spectrum of scintillation light, which is peaked around 520 nm.

The Lutetium-Yttrium garnets we have tested, have been kindly provided by SIC, where they are being developed mainly for applications as LED components. For this reason, they exhibit important fluorescence levels, that would need to be minimized for HL-LHC applications. The samples are visible in Fig. 2 , and a table of their characteristics is shown as Table 1.

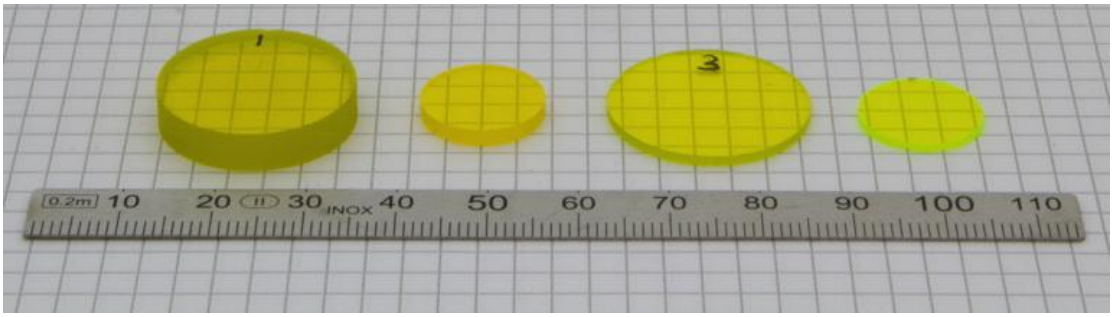

Figure 2: LuAG:Ce and YAG:Ce ceramic samples from SIC

Table 1: Characteristics of the tested ceramic garnet samples.

Label	Composition	$\varnothing$ [mm]	ℓ [mm]	ρ [g/cm^3]	X_0 [cm]
cYAG1	$Y_3Al_5O_{12}$	22.7	5.1	4.3	3.7
cYAG2	$Y_3Al_5O_{12}$	14.0	2.1	4.3	3.7
cLuYAG	$(Y,Lu)_3Al_5O_{12}$	23.4	1.3	5.5	2.1
cLuAG	$Lu_3Al_5O_{12}$	14.0	1.0	6.6	1.4

An example Light Transmissions for the YAG:Ce sample labeled cYAG1, before and after irradiation, is shown in Fig. 3. For all the samples, a broad color center is visible, that however affects the emission region in a modest way. For the sample of Fig.3, the induced absorption μ_{IND} does not exceed 1 m^{-1} over the entire range of emission wavelengths, between 520 and 560 nm. For the YAG:Ce sample cYAG2 and for LuYAG:Ce, the value stays below 10 m^{-1} and it remains smaller than 4 m^{-1} in LuAG:Ce.

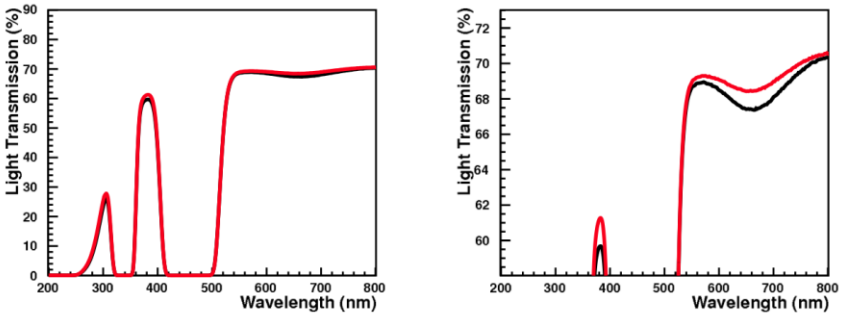

(a) for $200 < \lambda < 800$ nm. (b) zoomed detail

Figure 3: Light transmission for the ceramic YAG:Ce sample cYAG1 as a function of wavelength before (red) and after (black) irradiation with 24 GeV/c protons up to 10^{13} p/cm^2.

No recovery of damage has been observed over several months.

All these results are very promising, in terms of radiation hardness, and in terms of possibility of an economic manufacturing of inorganic scintillators, especially for sizes suitable in a sampling calorimeter. Detailed results have been published in [2.2-10].

5.5. BIBLIOGRAPHY

[2.2-1] M. Huhtinen, P. Lecomte, D. Luckey, F. Nessi-Tedaldi, F. Pauss, "*High-energy proton induced damage in $PbWO_4$ calorimeter crystals",* Nucl. Instrum. and Meth. A545 (2005) 63-87.

[2.2-2] P. Lecomte, D. Luckey, F. Nessi-Tedaldi, F. Pauss, "*High-energy proton damage study of scintillation light output from $PbWO_4$ calorimeter crystals",* Nucl. Instrum. and Meth. A564 (2006) 164-168.

[2.2-3] P. Lecomte, D. Luckey, F. Nessi-Tedaldi, F. Pauss, D. Renker, "*Comparison between high-energy proton and charged pion induced damage in $PbWO_4$ calorimeter crystals",* Nucl. Instrum. and Meth. A587 (2008) 266-271.

[2.2-4] G. Dissertori, D. Luckey, F. Nessi-Tedaldi, F. Pauss, R. Spikings, r. Van der Lelij, R. Wallny, *"A visualization of the damage in Lead Tungstate calorimeter crystals after exposure to high-energy hadrons",* Nucl. Instrum. and Meth. A684 (2012) 57-62.

[2.2-5] F. Nessi-Tedaldi on behalf of the CMS Collaboration, *Response Evolution of the CMS ECAL and R&D Studies for Electromagnetic Calorimetry at the High-Luminosity LHC,* paper N35-4, IEEE Nuclear Science Symposium (Anaheim, USA, 2012)

[2.2-6] A.S.Iljinov et al., Phys. Rev. C 39 (1989) 1420-1424.

[2.2-7] G. Dissertori, P. Lecomte, D. Luckey, F. Nessi-Tedaldi, F. Pauss et al., *"A study of high-energy proton-induced damage in Cerium Fluoride in comparison with measurements in Lead Tungstate calorimeter crystals",* Nucl. Instrum. and Meth. A622 (2010) 41-48.

[2.2-8] J.Chen et al., "*Gamma-ray induced radiation damage in large-size LSO and LYSO crystal samples",* IEEE Trans. Nucl. Sci. 54 (2007) 1319-1326.

[2.2-9] G. Dissertori, D. Luckey, F. Nessi-Tedaldi, F. Pauss, R. Wallny, "*Results on damage induced by high-energy protons in LYSO:Ce calorimeter crystals",* paper NP5.S-228, IEEE Nuclear Science Symposium (Valencia, Spain, 2011).

[2.2-10] G. Dissertori, M. Glaser, D. Luckey, F. Nessi-Tedaldi, F. Pauss, R. Wallny, "*Results on damage induced by high-energy protons in LYSO:Ce calorimeter crystals",* paper N1-133, IEEE Nuclear Science Symposium (Anaheim, USA, 2012).